Toward a theory of the general-anesthetic-induced phase transition of the cerebral cortex. II. Numerical simulations, spectral entropy, and correlation times

D. A. Steyn-Ross, Moira L. Steyn-Ross, and Lara C. Wilcocks
Department of Physics and Electronic Engineering, Private Bag 3105, University of Waikato, Hamilton, New Zealand

J. W. Sleigh
Department of Anaesthetics, Waikato Hospital, Hamilton, New Zealand

(Received 4 September 2000; revised manuscript received 10 February 2001; published 27 June 2001)

In our two recent papers [M.L. Steyn-Ross *et al.*, Phys. Rev. E **60**, 7299 (1999); 64, 011917 (2001)] we presented clinical evidence for a general anesthetic-induced phase change in the cerebral cortex, and showed how the significant features of the cortical phase change (biphasic power surge, spectral energy redistribution, ''heat capacity'' divergence), could be explained using a stochastic single-macrocolumn model of the cortex. The model predictions were based on rather strong ''adiabatic'' assumptions which assert that the mean-field excitatory and inhibitory macrocolumn voltages are ''slow'' variables whose equilibration times are much longer than those of the input ''currents'' that drive the macrocolumn. In the present paper we test the adiabatic assumption by running numerical simulations of the stochastic differential equations. These simulations confirm the number and nature of the steady-state solutions, the growth of fluctuation power at transition, and the redistribution of spectral energy towards lower frequencies. We use spectral entropy to quantify these changes in the power spectral density, and to show that the spectral entropy should decrease markedly at the point of transition. This prediction agrees with recent clinical findings by Viertiö-Oja and colleagues [J. Clinical Monitoring Computing **16**, 60 (2000)]. Our modeling work shows that there is an inverse relationship between spectral entropy H and correlation time T of the soma-voltage fluctuations: $H \propto -(\ln T)$. In a theoretical analysis we prove that this proportionality becomes exact for an ideal Lorentzian process. These findings suggest that by monitoring the changes in EEG correlation time, it should be possible to track changes in the state of patient consciousness.

DOI: 10.1103/PhysRevE.64.011918 PACS number(s): 87.19.La, 05.10.Gg, 05.70.Fh

I. INTRODUCTION

Our two earlier papers [1] and [2] introduced a theoretical model to describe the gross changes in EEG (electroencephalogram) characteristics observed when a patient undergoes general anesthesia. In order to make the model equations amenable to analytic treatment it was necessary first to find the stationary states of the model, then to make an adiabatic approximation in which it is assumed that the h_e (excitatory) and h_i (inhibitory) soma voltages of the mean-field macrocolumn vary on time scales much slower than those of the input ''currents'' which are integrated by the macrocolumn capacitor. This simplification allowed us to calculate a theoretical fluctuation spectrum for small white-noise perturbations of the macrocolumn about its steady state, and to predict how this spectrum would change as a function of anesthetic concentration.

To verify the correctness of the theoretical analysis of papers [1,2], we deemed it essential to run numerical simulations of the stochastic differential equations, and it is the first task of the present paper to report in Sec. II the results of these numerical experiments. Specifically, these experiments (i) confirm the predicted number, character, and locations of the macrocolumn steady states as a function of anesthetic effect; (ii) give a numerical demonstration of the growth in fluctuation power (the ''biphasic effect'') as the conscious $\rightarrow$unconscious transition point is approached; and (iii) establish the range over which the adiabatic and full equations give similar results, and identify the point at which their behaviors are expected to diverge.

We find that the spectral power of the EEG redistributes towards lower frequencies as the anesthetic effect increases. This redistribution can be quantified in terms of the *Shannon spectral entropy* (defined later in the paper), giving a measure of the flatness (''whiteness'') of the EEG spectrum. In Sec. III we compare the theoretical and numerical predictions for the anesthetic-driven change in spectral entropy, then test these model predictions against clinical measurements furnished by Viertiö-Oja and colleagues [3]. We find good qualitative agreement between model results and clinical measurement for spectral entropy change during induction of general anesthesia.

These changes in the macrocolumn spectral response should also be detectable in the time domain. As pointed out in [1], the model predicts there will be a pair of distinct first-order phase transitions: one at the A_3 conscious $\rightarrow$unconscious induction (see Fig. 5 of [1]), and another at the Q_1 unconscious$\rightarrow$conscious emergence return. We would expect both of these transitions to be heralded by a significant lengthening of the correlation times (the so-called ''critical slowing down'') of the soma-voltage fluctuations as the macrocolumn jump points are approached. We demonstrate that the model correlation times do evolve in this way, but we have not yet applied this time-domain analysis to real EEG data.

In the final part of Sec. III we investigate the link between spectral entropy and correlation time for the soma-voltage

fluctuations, and find that the two quantities appear to be inversely related: spectral entropy scales as the negative logarithm of the correlation time. We comment on a possible clinical application of this finding.

II. NUMERICAL VERIFICATIONS OF THE THEORY

A. Simulating the stochastic differential equations

The macrocolumn equations of motion for the excitatory and inhibitory soma voltages consist of a set of eight coupled stochastic differential equations: two first-order, six second-order; the stochastic differential equations (SDEs) are given in Eqs (2.1)–(2.4) of [2]. After replacing each second-order differential equation (DE) with a pair of first-order DEs, we can write down a set of 14 first-order difference equations which can then be integrated with an Euler one-step scheme. We refer to this 14-equation set as the *full, nonadiabatic* equations.

We can greatly simplify the equation set by making the adiabatic assumption (i.e., that the $h_{e,i}$ soma voltages are ''slow'' variables which equilibrate on much longer time scales than the I_{jk} input currents). This gives a single pair of coupled first-order Langevin equations listed as Eqs. (2.9) and (2.10) in [2]. Rewriting these as difference equations, the soma voltages evolve as the sum of drift $F\Delta t$ and diffusion $\Gamma\Delta t$ terms,

$$h_e^{n+1} = h_e^n + F_1^n \Delta t + \Gamma_e^n \Delta t, \tag{2.1a}$$

$$h_i^{n+1} = h_i^n + F_2^n \Delta t + \Gamma_i^n \Delta t, \tag{2.1b}$$

where the superscript n means ''value at time step n,'' and Δt is the time increment. The $F_{1,2}^n$ are the simulated drift terms which are straightforward discretizations of the continuous-time drift equations (2.10a) and (2.10b) of [2]. The discretization of the diffusion equations (2.10c) and (2.10d) of [2], $\Gamma_{e,i}$ requires some care; the resulting equations are

$$\Gamma_e^n = \left\{ \psi_{ee}(h_e^n)\alpha_{ee}\sqrt{\langle p_{ee}\rangle}\frac{\mathbb{R}_1^n}{\sqrt{\Delta t}} G_e e/\gamma_e + \lambda\psi_{ie}(h_e^n)\alpha_{ie}\sqrt{\langle p_{ie}\rangle}\frac{\mathbb{R}_3^n}{\sqrt{\Delta t}} G_i e/\gamma_i \right\} \Big/ \tau_e, \tag{2.2a}$$

$$\Gamma_i^n = \left\{ \psi_{ei}(h_i^n)\alpha_{ei}\sqrt{\langle p_{ei}\rangle}\frac{\mathbb{R}_2^n}{\sqrt{\Delta t}} G_e e/\gamma_e + \lambda\psi_{ii}(h_i^n)\alpha_{ii}\sqrt{\langle p_{ii}\rangle}\frac{\mathbb{R}_4^n}{\sqrt{\Delta t}} G_i e/\gamma_i \right\} \Big/ \tau_i. \tag{2.2b}$$

(Symbols are as defined in Table I of [2].) There are two points of note here. First, each of the four independent, δ-correlated, infinite-variance white noise sources $\xi_{k,k\in\{1\ldots4\}}$ of [2] have been replaced in the simulation equations by their discrete approximation $\mathbb{R}_k/\sqrt{\Delta t}$ where the $\mathbb{R}_k$ are independent, Gaussian-distributed sources of random numbers with mean zero, variance unity. The division by $\sqrt{\Delta t}$ ensures that the diffusion increment $\Gamma\Delta t$ scales as the square root of the time step as required for a Wiener process [4,5].

Second, the $\alpha_{jk(j,k\in\{e,i\})}$ are constant dimensionless safety factors designed to ensure that the random fluctuations in the p_{jk} subcortical inputs always remain small. The appropriate setting depends on the size of the time step. For our simulations, we set $\Delta t = 10^{-4}$ s and $\alpha_{jk} = 0.1$. This value for the safety factor ensured that there would be negligible probability that a fluctuation in p_{jk} would ever exceed its $\langle p_{jk}\rangle$ average value.

To start the integration, the initial values for soma voltages h_e and h_i typically would be set equal to their zero-noise equilibrium values, derived from Fig. 1 of [2], appropriate to the given value of anesthetic effect λ:

$$h_e^0 = h_e^{\text{eq.}}(\lambda), \quad h_i^0 = h_i^{\text{eq.}}(\lambda).$$

For λ in the range $0.28 < \lambda < 1.53$, the equilibrium curve has a multivalued ordinate, so we would select either the top-, middle-, or bottom-branch $(h_e^{\text{eq.}}, h_i^{\text{eq.}})$ equilibrium values, depending on the particular numerical experiment we wished to run.

B. Verification of macrocolumn steady states

The theoretical equilibria determined in [1] were verified by running numerical simulations of both the full 14-equation nonadiabatic set and of the adiabatically simplified two-equation set. These simulation runs showed that the steady-state values calculated in [1] are correct, that the upper and lower branches are stable (with the exception of the high-λ top branch for the full equations; this is discussed below), and that the middle branch is unstable. We demonstrated this by starting the system on the middle (unstable) equilibrium point. The macrocolumn would never sit there, but would ''fall'' off the potential hill, settling into either the upper-branch (high-firing) equilibrium valley, or the lower-branch (low-firing) equilibrium valley. The ''splitting probability'' (i.e., the probability of falling into a given valley) was found to be $\sim 50\%$. See Figs. 1 and 2.

Figure 1 shows that the adiabatic runs settle to one of the stable states within about 200 samples (20 ms). It appears that the time required to settle decreases with increasing λ. Figure 2 illustrates the much slower evolution of the full equations, typically taking an order of magnitude longer (2000 samples, 200 ms) than the adiabatic equations to settle to steady state. We also see that for $\lambda = 1.3$ [Fig. 2(c)], unlike the adiabatic case, the full-equation upper branch is *unstable*: all runs which go to the upper branch develop an exponentially growing oscillation about that branch before collapsing to the bottom branch.

To discover the source of this instability we performed a linear stability analysis of the full equation set, and found that, on the top branch, the real part of the dominant eigenvalue goes positive when the anesthetic parameter $\lambda > 1.2$. Subsequent simulation runs confirmed this finding: the upper branch is only stable in the full-equation case for $\lambda < 1.2$. As λ approaches this value from below, the simulations show an

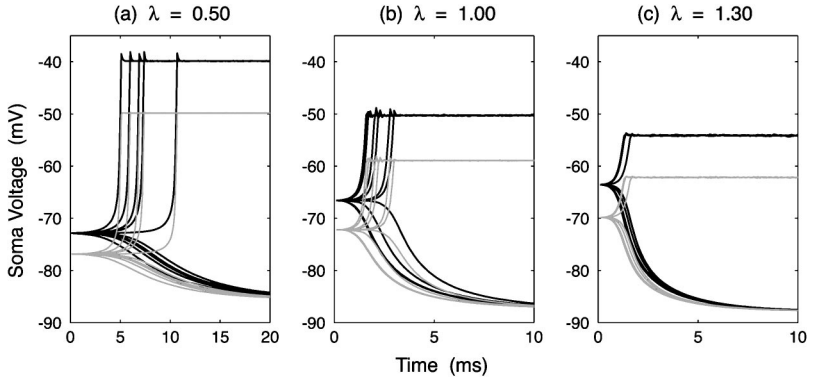

FIG. 1. Settling to steady state for stochastic simulations of the adiabatic equations for three values of the anesthetic effect lying within region II of the S-bend (see Fig. 1 of [2]): (a) $\lambda = 0.5$; (b) $\lambda = 1.0$; (c) $\lambda = 1.3$. The four random noise sources to the p_{jk} subcortical spike inputs each have amplitude $\alpha = 0.1$. The time step is 0.1 ms. The dark (light) curves show time evolution for h_e (h_i). For each λ value, ten independent runs are shown. Each run is started on the unstable (h_{e_0}, h_{i_0}) equilibrium point at the crest of the potential hill separating the two valleys (see Fig. 4 of [2]), but cannot remain there. Random fluctuations cause the soma voltages to roll off the hill into either valley with equal probability. The upper stable equilibrium is the high-firing, active state; the lower stable equilibrium is the hyperpolarized, quiescent state.

increasingly undamped oscillation at ~10 Hz (the so-called EEG α-band resonance). However, a time-frequency analysis of clinically measured EEG wave forms does *not* show a preferential growth of α-band power during anesthetic induction. Instead, the clinical traces show a broad transfer of power from higher to lower frequencies as the induction point is approached, just as predicted by the simpler, adiabatic theory (see Fig. 6 of [1], and Figs. 4 and 5, discussed later in this paper).

Resonances are absent in our adiabatic theory because the adiabatic approximation eliminates the second-order time derivatives that appear in the full equations. While the full equations have a very rich range of dynamic behaviors similar to EEG patterns observed in the conscious cerebral cortex, for the purposes of modeling anesthetic induction, the simpler, adiabatic theory seems to provide a better match with clinical measurement. For this reason, the present paper focuses on the adiabatic predictions.

C. Verification of fluctuation divergence (biphasic power surge) at induction

Figures 6 and 7 of [1] illustrated the linearized adiabatic-theory prediction of a dramatic increase in low-frequency fluctuation power as the conscious → unconscious transition is approached. Within the anesthesiology community, this power surge is referred to as the ''biphasic'' or activation-depression response to general anesthetic [6–8]. Here, we verify that numerical simulation also shows a biphasic response: the adiabatic equations produce an h_e time series whose fluctuations about steady state grow strongly as the macrocolumn nears its λ_{A_3} transition point.

The adiabatic macrocolumn is started at $\lambda = 0.3$ on the upper branch of the S curve (see Fig. 1 of [2]). During a 30-s simulation run, the anesthetic effect is slowly and steadily increased to reach a final value of $\lambda = 2.3$ after 300 000 iterations for a time step $\Delta t = 10^{-4}$ s. The simulation results in

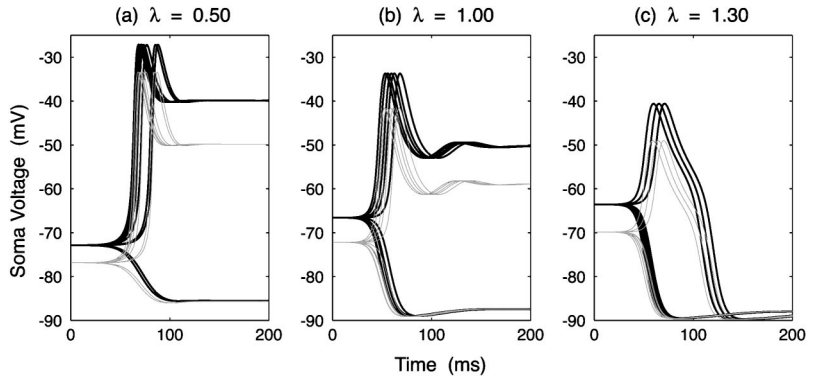

FIG. 2. Stochastic simulation results for full (nonadiabatic) equations for (a) $\lambda = 0.5$; (b) $\lambda = 1.0$; (c) $\lambda = 1.3$. Initial settings and noise amplitudes are as in Fig. 1. Full-equation runs generally demonstrate the same steady-state asymptotes as the adiabatic runs, but note that settling times are an order of magnitude longer here, and the upper branch is now characterized by an oscillatory dynamic, of frequency ~10 Hz, which is strongly damped for small λ, but becomes much less damped as λ is increased. For $\lambda \gtrsim 1.3$, the oscillation about the upper branch becomes so strong that the upper equilibrium becomes dynamically unstable, causing trajectories originally headed towards the high-firing branch to deviate and collapse into the hyperpolarized quiescent branch.

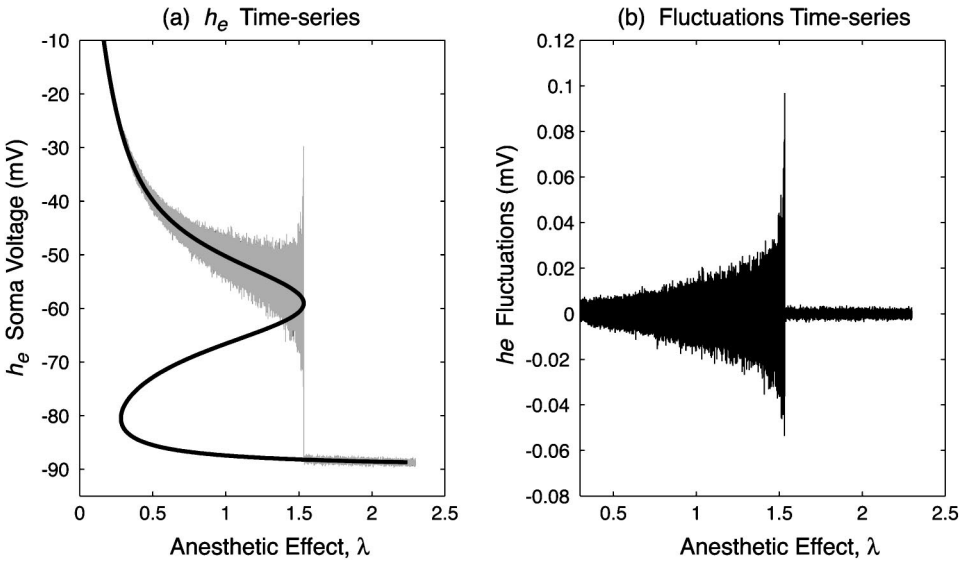

FIG. 3. Time series of excitatory soma potential h_e for induction into unconsciousness. (a) Time development along the equilibrium curve; (b) ac fluctuations residual after subtraction of the dc equilibrium component. The h_e time series was generated by a 30-s adiabatic simulation run in which λ was steadily increased from 0.3 to 2.3 during the course of the run. Time step: $\Delta t = 0.1$ ms for 300 000 samples; noise scale $\alpha = 0.1$. In (a), the fluctuations are displayed at 300× actual size in order to make them visible on the equilibrium voltage scale. Their true scale is shown in (b).

Fig. 3 show a flaring cornucopia of soma-voltage fluctuations that reach their maximal extent at the moment of transition, then abruptly collapse immediately after the jump to the much lower values characteristic of a low-firing, hyperpolarized macrocolumn.

This divergent growth in fluctuation power is reminiscent of the divergent behavior observed in many physical phase transitions, supporting that notion that the conscious ↔ unconscious transition can be analyzed as a physical change of state.

D. Verification of EEG spectral changes

1. Predictions of adiabatic theory

The theoretical fluctuation spectra were computed by linearizing the adiabatic equations about the S-bend (Fig. 1 of [2]) steady state (found by setting all derivatives and noise terms to zero). This produced a pair of linearized stochastic differential equations for the variations in the soma voltages $\tilde{h}_{e,i}$ about steady state, from which the stationary fluctuation spectrum is derived as

$$\mathcal{S}[h_e(\omega)] = \frac{1}{2\pi} \frac{D_{11}A_{22}^2 + D_{22}A_{12}^2 + D_{11}\omega^2}{(A_{11}A_{22} - A_{21}A_{12} - \omega^2)^2 + (A_{11} + A_{22})^2\omega^2}. \tag{2.3}$$

The four drift-matrix elements A_{11}, A_{12}, A_{21}, and A_{22} are as listed in the Appendix equations (A1)–(A4) of [1] [but note the small typographical error on the last line of Eq. (A4) of [1]: the postsynaptic amplitude term is incorrectly subscripted, and should read G_i (not G_e)].

As explained in Sec. II A, in order for simulation to match theory, the four subcortical noise inputs must be kept sufficiently small, necessitating the introduction of scaling factors $\alpha_{jk}\sqrt{\langle p_{jk}\rangle}$ which multiply the four white-noise terms [see Eq. (2.5) of [2]]. This means that the two diffusion-matrix elements D_{11} and D_{22} listed in the Appendix equations (A5) and (A6) of [1] require modification, and now read

$$D_{11} = \frac{1}{\tau_e^2}\{(\psi_{ee}\alpha_{ee}G_e e/\gamma_e)^2\langle p_{ee}\rangle + \lambda^2(\psi_{ie}\alpha_{ie}G_i e/\gamma_i)^2\langle p_{ie}\rangle\}_{\rm eq}, \tag{2.4}$$

$$D_{22} = \frac{1}{\tau_i^2}\{(\psi_{ei}\alpha_{ei}G_e e/\gamma_e)^2\langle p_{ei}\rangle + \lambda^2(\psi_{ii}\alpha_{ii}G_i e/\gamma_i)^2\langle p_{ii}\rangle\}_{\rm eq}. \tag{2.5}$$

Figure 4 shows how the theoretical spectrum changes as a function of anesthetic effect λ. There are two significant features. First, there is a very obvious surge in fluctuation power as the induction [Figs. 4(a) and 4(b)] and emergence [Figs. 4(c) and 4(d)] transition points are approached. This power surge is the anesthetic biphasic peak referred to earlier, and was seen in the simulation time series also (Fig. 3).

Second, there is a marked change in the spectral distribution of the fluctuation power. As transition is approached along the top branch, the spectrum changes from being fairly flat to having a strong roll-off characteristic with a peak at zero frequency. This tendency towards zero-frequency peakiness is even more pronounced for the emergence path [Figs. 4(c) and 4(d)]. This alteration in spectral shape is the basis of the changes in spectral entropy and correlation time discussed later.

2. Adiabatic simulation spectra

The simulation spectra were computed by Fourier transforming the pseudo-EEG wave forms generated by iterating the coupled adiabatic equations of motion [Eqs. (2.1)] for the excitatory and inhibitory soma voltages. We would start the adiabatic macrocolumn at the upper- or lower-branch stable equilibrium point corresponding to a given value of λ, then induce fluctuations about steady state by driving the macrocolumn subcortical inputs with four independent white-noise sources. Each run consisted of 100 000 iterations with a time-step $\Delta t = 10^{-4}$ s, giving a 10-s pseudo-EEG record.

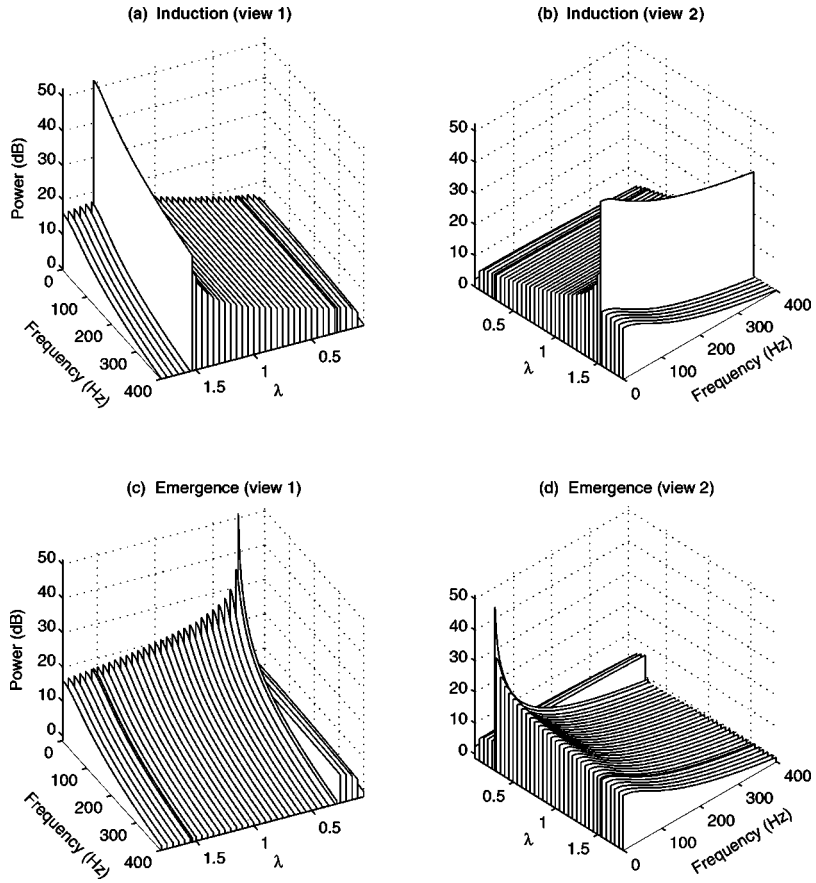

FIG. 4. Theoretical prediction for the variation of spectral power for [(a) and (b)] anesthesia induction (path $A_1A_3Q_3C$ of Fig. 1 in [2]), and for [(c) and (d)] the emergence from anesthesia ($Q_3Q_1A_1$). Two views are shown for each trajectory to allow visual comparison of the relative flatness (''whiteness'') of the spectral curves before and after transition. Note the slab of biphasic power which heralds the slump into unconsciousness at the $A_3 \rightarrow Q_3$ transition in (a) and (b). There is a similar increase in cortical power on the return journey as the macrocolumn emerges from unconsciousness, with total power rising to a peak immediately prior to the $Q_1 \rightarrow A_1$ jump to the upper branch.

This was repeated for λ values ranging from 0.3 to 1.8 in steps of 0.1. The resulting adiabatic simulation spectra are shown in Fig. 5.

For frequencies below 400 Hz, agreement between theory and simulation is excellent. At higher frequencies, the simulation spectra overestimate the theoretical result, particularly when the macrocolumn is predicted to have a relatively flat spectral response [e.g., $\lambda = 0.3$ and $\lambda = 1.0$ on the top branch: see Figs. 5(a) and 5(b)]. Agreement at high frequencies is more convincing in those cases for which the macrocolumn is predicted to have a strongly low-pass filtering characteristic [Figs. 5(c)–5(f)]. This is explicable as an aliasing artifact in the simulation arising from the fact that the macrocolumn is being driven by unfiltered white noise, so the only ''anti-aliasing protection'' in the sampled pseudo-EEG time series is that provided by the low-pass filtering characteristics of the macrocolumn itself. We have verified that if we lower the maximum excitatory and inhibitory firing rates by a factor of 10 from the present (physiologically rather high) values of $S_{e,\max} = S_{i,\max} = 1000\ \mathrm{s}^{-1}$ (see Table I of [2]) to $100\ \mathrm{s}^{-1}$, then the -3-dB frequency for the power spectrum reduces by about an order of magnitude, and the aliasing error is much reduced.

We also computed the total fluctuation power in the range dc to 5000 Hz and dc to 400 Hz by summing the area of the 1-Hz histogram bins. The comparisons between simulation and prediction are shown in Fig. 6. The biphasic power peaks demarking the induction and emergence transition points are of similar magnitude for both frequency bands, indicating that most of the fluctuation power near transition resides in the lower frequencies. We observe that the agreement between simulation and theory is excellent for the 0–400-Hz band [Fig. 6(b)], but degraded for the 0–5000-Hz band [Fig. 6(a)] for the upper branch where aliasing errors are likely to be most apparent.

3. Nonadiabatic simulation spectra

As mentioned earlier, numerical simulations of the full 14-equation model showed that the nonadiabatic macrocolumn becomes unstable along the upper branch for $\lambda > 1.3$. Unlike the adiabatic case, small soma-voltage fluctuations about the upper-branch steady state would evolve into a $\sim$10-Hz oscillation whose amplitude would grow inexorably until the macrocolumn collapsed ''early'' to the low-firing-rate lower branch, whereupon the oscillations would vanish. This numerical finding was confirmed by a linear stability

analysis of the nonadiabatic equations which showed that along the top branch, one of the 14 eigenvalues has a real part which goes positive when $\lambda > 1.3$, causing this high-λ regime to become unstable. It is therefore not possible to define a steady-state fluctuation spectrum for the high-λ regime using the full equations, since the deterministic growth completely swamps the stochastic behavior. Fuller investigation of the full-model equations is deferred to a later paper.

III. ENTROPY CONSIDERATIONS: STATISTICS, THERMODYNAMICS, AND SPECTRA

A. Entropies for the macrocolumn

An implicit assumption in our work is that the model behavior of a single macrocolumn of $\sim 10^5$ cooperating neurons can serve as a proxy for the bulk behavior of the $\sim 10^6$ macrocolumns comprising the $\sim 10^{11}$ neuron population of the cortex. This ''one speaks for all'' macrocolumn picture is probably not too unreasonable when applied to the task of characterizing the gross changes that occur when there is a massive switchover in cortical function from active-consciousness to comatose-unconsciousness. After all, these gross changes can be, and routinely are, detected using a single EEG electrode which is only sampling $\sim 1\%$ of the total macrocolumn population. In our companion paper [2] we proposed that this gross change in state could be quantified in terms of an ''anestheto-dynamic entropy'' defined as the negative rate of change of macrocolumn free energy with respect to its excitability Θ, $S = -dV/d\Theta$.

Another means for quantifying the state of orderliness of the cortex would be to apply a statistical mechanics formalism which defines entropy in terms of Ω, the statistical weight of the macrostate (i.e., the number of *micro*states equivalent to the given macrostate), $S_\Omega = k_B \log_e \Omega$, where k_B is Boltzmann's constant. S_Ω is a measure of the availability or spread of the microstates, indicating their degree of randomness or disorder. For the macrocolumn picture, a microstate is one particular depolarized and/or hyperpolarized electrical configuration of the 10^5 neurons within the macrocolumn. The weight for this microstate would be the number of distinct voltage configurations of the 10^5 excitatory and inhibitory neurons, whose net effect, when summed over the whole macrocolumn, is to produce a given excitatory and inhibitory (h_e, h_i) voltage ''coordinate.'' The equilibrium state for a given value of anesthetic effect would then be that state which maximized the number of available microstates.

Our model has no detailed knowledge of the state of its constituent neurons, so it cannot be used to count microstates (except perhaps for the fully hyperpolarized state of extreme coma: in this case all neurons are assumed to be in the same zero-firing state at -90 mV, giving a microstate count of unity). Clinical measurements of scalp-detected EEG are also unable to reveal microscopic details of the individual neuron states. This is because the recordings are the summation of the electrical activity of the several thousand macrocolumns in the vicinity of the electrode: all internal microstate structure has been irretrievably blurred out by the spatial and temporal averaging.

Despite the fact that knowledge of the internal microstate structure is unavailable to us, our simple macrocolumn model has demonstrated considerable predictive utility with respect to the anesthetic transition, indicating that the model equations provide a not unreasonable coarse-grained picture of the bulk behavior of the cerebral cortex. This leads us to ask: Can the model be used to infer some of the internal physics of the brain from the external EEG signal? Specifically, can we uncover and quantify the link between the externally measurable EEG *spectral* entropy (defined below) and the internal state of disorder of the cerebral cortex during the transition into unconsciousness?

That there is a link between EEG and brain state is well established. For example, Steriade *et al.* [9] observe the following: ''The rapid patterns characteristic of the aroused state are replaced by low-frequency, synchronized rhythms of neuronal activity when the brain falls asleep.'' So, the unconscious brain has a relatively simple EEG spectrum, whereas the spectrum for the conscious brain is noisier and more complex. EEG complexity can be quantified in frequency space by way of the *Shannon spectral entropy* defined as [10,11]

$$H = -\frac{1}{\ln N} \sum_{i=1}^{N} p_i \ln p_i , \tag{3.1}$$

where i is a frequency index and p_i is a normalized spectral density

$$p_i = \frac{\mathcal{S}(\omega_i)}{\sum_{j=1}^{N} \mathcal{S}(\omega_j)}, \tag{3.2}$$

giving the probability of occupation of the ith bin of an N-bin histogram for the power spectrum $\mathcal{S}(\omega)$. Spectral entropy H measures the relative flatness (''whiteness'') of the spectrum. H has a maximum value of unity for a perfectly flat spectral histogram, and has a diminished positive value for a spectrum which has resonance peaks or which follows a decay law (e.g., power $\sim 1/f^n$).

As shown in [2], our phase-transition model for the cortex suggests that the anestheto-dynamic entropy (i.e., analogous thermodynamic entropy) will be smaller in the hyperpolarized (unconscious) state. Since the cortex will have fewer microstates available to it in this well-ordered state, its firing behavior and resulting EEG spectrum should be relatively simple, so it is reasonable to expect that spectral entropy H should also be smaller in the unconscious state. Conversely, both kinds of entropy should be larger in the relatively disordered, more complex active state. Thus we expect changes in the spectral entropy to track changes in the internal thermodynamic entropy, providing an external measure of the internal state of the cortex.

In the next section we investigate how the spectral entropy of the adiabatic macrocolumn is expected to vary with the anesthetic effect, using numerical simulations to check the theoretical predictions. We compare our model results with clinical determinations of spectral entropy reported by

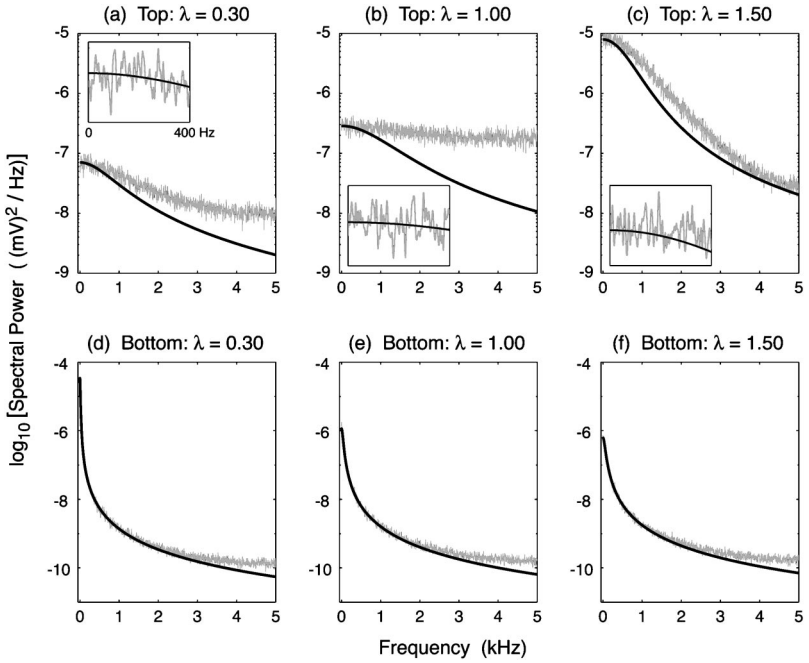

FIG. 5. Comparison of theoretical fluctuation spectra (black curves) with stochastic simulation spectra (gray curves) for the adiabatic equations. (The noise amplitudes and time step are as for Fig. 1.) Simulation graphs were computed as the averaged spectra for ten 1-s time-series segments (10 000 samples per segment) which were then smoothed with a 5-point moving-average filter. Plots (a)–(c) are fluctuation spectra for three representative anesthetic values on the top (high-firing) branch; plots (d)–(f) are the corresponding spectra for the bottom (low-firing, quiescent) branch. At low frequencies, agreement between theory and simulation is excellent [see the inset graphs for 0–400-Hz detail in (a)–(c)]. At higher frequencies, the simulation spectra become inaccurate; this is an inevitable consequence of driving the macrocolumn with unfiltered Gaussian noise sampled at 10 kHz, producing aliasing artifacts. Aliasing errors diminish when the macrocolumn has a strong low-pass filtering characteristic (e.g., the bottom branch: (d)–(f), and the top branch near transition: (c)], but become significant when the macrocolumn frequency response is relatively flat.

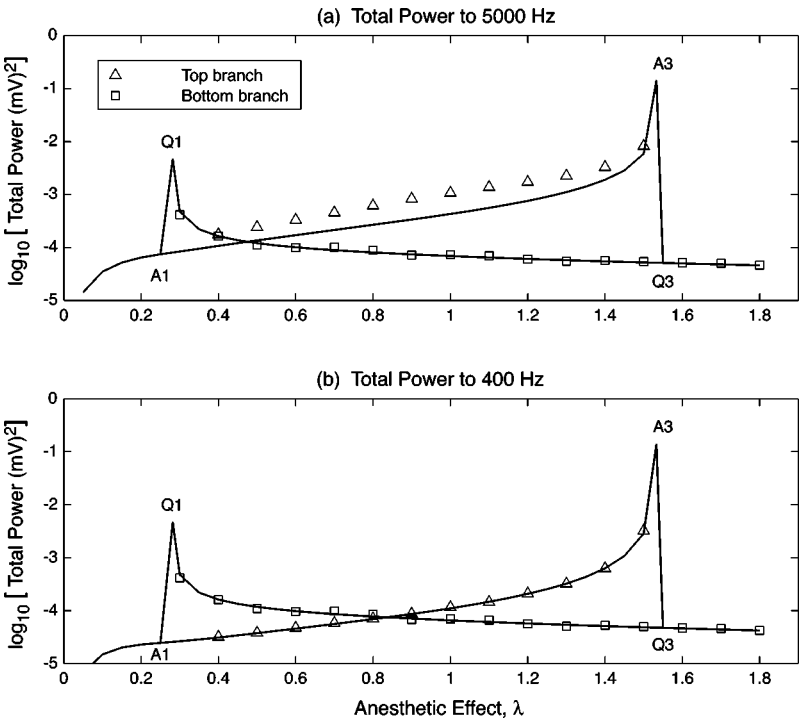

FIG. 6. Total fluctuation power (a) to 5000 Hz, (b) to 400 Hz for the macrocolumn as a function of the anesthetic effect; solid lines: theoretical prediction; points: simulation results. Curves show the predicted trends in fluctuation power computed from the area under the theoretical spectral density curves of Fig. 4. Points are obtained from the power spectra of the pseudo-EEG h_e time series generated by numerical simulation of the adiabatic equations (time step $\Delta t = 0.1$ ms; noise scale factor $\alpha = 0.1$). Total power was estimated by summing into 1-Hz bins the area under the power spectral density curves from 0–5000 Hz (a) and 0–400 Hz (b).

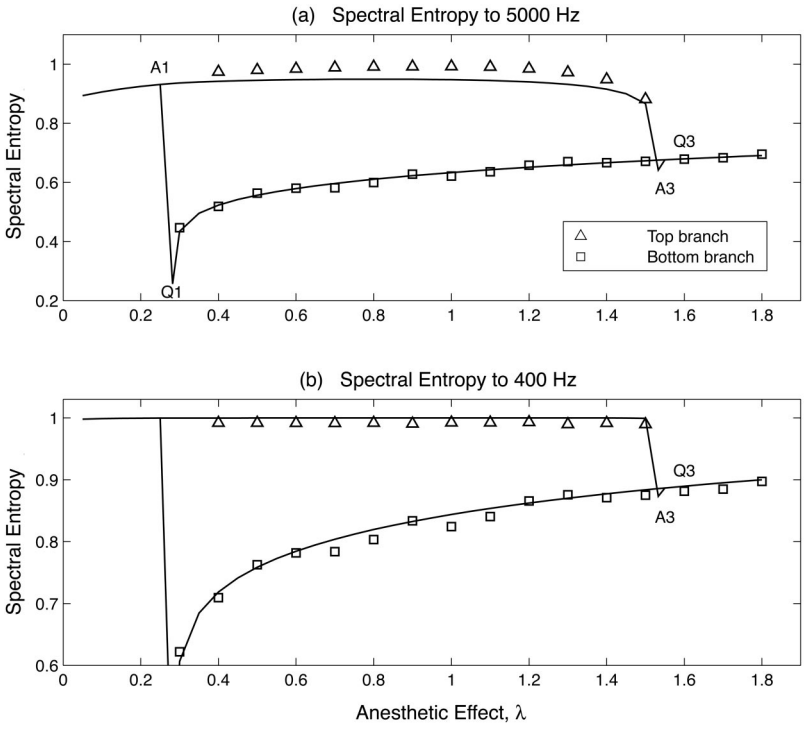

FIG. 7. Theoretical prediction and simulation results for Shannon spectral entropy for (a) 0–5000 Hz, (b) 0–400 Hz; solid lines: prediction; discrete points: simulation results. Spectral entropy is typically high on the upper (active) branch, and low on the quiescent branch. For induction into unconsciousness, spectral entropy declines steeply but continuously. In contrast, during emergence into consciousness the spectral entropy makes a discontinuous upwards jump at transition. The points labeled A_3 and Q_1 mark the cusps in fluctuation power that occur at the instant preceding induction into unconsciousness and emergence from unconsciousness, respectively.

Viertiö and colleagues [3] for patients undergoing general anesthesia. We then look for a relationship between spectral entropy and fluctuation correlation time, and find a direct logarithmic mapping between these frequency- and time-domain measures.

B. Spectral entropy prediction from adiabatic theory

Using the theoretical adiabatic fluctuation spectra calculated from Eq. (2.3), we computed the normalized Shannon spectral entropy [Eq. (3.1)] with 1-Hz histogram bins for frequency ranges 0–5000 Hz and 0–400 Hz. See Fig. 7. For both frequency bands, the spectral entropy is higher on the upper (active) branch and lower on the bottom (quiescent) branch. This is consistent with the notion that spectral entropy will be large when the spectrum is relatively flat or ''white'' (all frequency bins equally populated), and small for a peaked spectrum (low-frequency bins more favored than high-frequency bins). As the three-dimensional (3D) plots in Fig. 4 show, for small values of λ the shape of the adiabatic power spectra for the top branch is considerably flatter than for the bottom branch. As $\lambda \to 1.53$ along the top branch, the total fluctuation power rises to a peak, but its spectral distribution becomes increasingly concentrated towards lower frequencies, so the spectral entropy decreases to a local minimum at the A_3 critical point immediately prior to the $A_3 \to Q_3$ induction jump.

For the Q_3Q_1 emergence trajectory along the bottom branch, the fluctuation spectra become even more dc-peaked, hence the steep decline in spectral entropy in anticipation of the $Q_1 \to A_1$ jump return to the upper branch.

Also shown in Fig. 7 are the spectral entropy values calculated from the spectra derived from the adiabatic time-series. Agreement between theory and numerical experiment is generally very good. We found that the nonadiabatic spectral entropy curves (not shown here) differ markedly from the adiabatic ones: this is because the spectral entropy values are diminished by the appearance of α-band resonances on the upper branch which tend to swamp the stochastic trends.

C. Spectral entropy from clinical measurements

We have recently become aware of clinical research by Viertiö-Oja and colleagues [3] investigating the feasibility of using spectral entropy of patient EEG as a robust measure of depth of anesthesia. 105 patients undergoing routine general anesthesia were monitored using 12-lead EEG. The state of consciousness was manually scored by an expert observer using the six-level OAAS scale (observer's assessment of alertness and sedation: 5 = fully awake; 0 = deep anesthesia). Loss of consciousness is defined as the transition from OAAS 3 to OAAS 2. After the transition, the patient no longer responds to spoken commands and the eyelid reflex is lost.

The OAAS scores were compared with the EEG spectral entropy values, and it was found that the entropy tracked the anesthesiologist's rating, with loss of consciousness occurring at a universal critical value of entropy which was found to be independent of the patient. Figure 8 illustrates the strong correlation between the EEG measure and the observer assessment of consciousness.

Comparing the clinical results against the adiabatic prediction of Fig. 7, there is good qualitative agreement for the induction trajectory: adiabatic spectral entropy declines as the macrocolumn transits from the high-firing upper branch to the low-firing quiescent branch; this parallels the decline in clinical spectral entropy as the patient becomes anesthetized. In both cases, the rate of decline is steepest at transition.

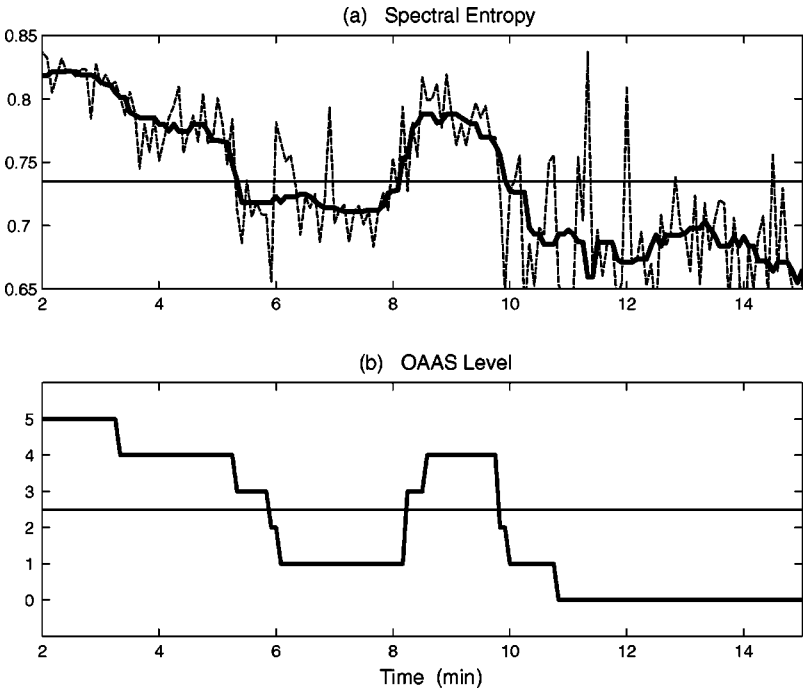

FIG. 8. (a) Spectral entropy derived from patient scalp EEG during the induction of anesthesia. The dashed curve shows 5-s averages; the heavy curve shows 1-min median-filtered averages. The EEG was sampled at 10 000 s^{-1}, decimated to 500 s^{-1}, and processed in 5-s segments. For each segment, spectral entropy was calculated using a frequency-histogram binwidth of 0.2 Hz. (b) The OAAS (observer's assessment of alertness and sedation) level as assessed by an anesthesiologist. Level 5 is fully awake; level 0 is a deep hypnotic state in which the patient shows no response to tetanic stimulation of the ulnar nerve (50 mA, 5 s). In both figures, the horizontal line shows the level at which transition from consciousness to unconsciousness occurs (OAAS 3 $\rightarrow$ 2). (Data supplied courtesy H. Viertiö-Oja, and reported as patient 75 in Ref. [17]).

However, theory and experiment diverge for the emergence trajectory. The adiabatic theory predicts that once the macrocolumn has reached the low-firing branch, reducing the anesthetic concentration should lead to ever-diminishing spectral entropy as the macrocolumn approaches the Q_1A_1 critical point from the right, yet the clinical measurements seem to bottom-out at a minimum value of ~ 0.66.

A possible explanation for this discrepancy might be that the stochastic fluctuations for the bottom-branch macrocolumn are expected to be very much smaller than for the top branch (compare the ''before'' and ''after'' fluctuation amplitudes of Fig. 3), consequently the stochastic component of the unconscious cortex could easily be swamped by any broad-band cortical resonances generated by the relatively ordered macrocolumns of the hyperpolarized cortex. If this is so, it may provide a means of distinguishing the stochastic and nonstochastic components of the EEG signal by looking for transition-induced changes in the characteristics of the autocorrelation function of the EEG time-series.

D. Correlation time and its relationship to spectral entropy

The theoretical fluctuation spectrum is approximately Lorentzian. This can be seen by considering the high-frequency limit of Eq. (2.3),

$$\mathcal{S}(\omega) \rightarrow \frac{1}{2\pi} \frac{D_{11}}{\omega^2 + (A_{11}+A_{22})^2}. \tag{3.3}$$

This approximation will become more accurate as the point of transition is approached and the spectrum narrows and rises. We can identify the constant term $(A_{11}+A_{22})$ in the denominator as a relaxation rate, and its inverse as a correlation time $T=1/(A_{11}+A_{22})$. The inverse-Fourier transform of the power spectrum gives the autocorrelation function (this is the Wiener-Khinchin theorem). For the Eq. (3.3) ideal Lorentzian spectrum, the autocorrelation function will be an exponentially decaying function of time,

$$\langle h_e(t) h_e(0) \rangle = \frac{1}{2} D_{11} T e^{-|t|/T}, \tag{3.4}$$

which will broaden at the induction and emergence transition points as the spectrum narrows, becoming more dc-peaked as the time scale for the voltage fluctuations increases. This is the classical ''critical slowing down'' phenomenon observed in phase transitions. (A similar description relating changes in spectral shape to changes in correlation time has been given by Shenoy in his treatment of the driven Josephson junction as an analog of optical bistability [12].)

Is there a relationship between spectral entropy and correlation time for the fluctuations? The adiabatic theory suggests that there is, and that it is inverse. As the fluctuation spectrum narrows and rises on approach to transition, the spectral entropy decreases (the spectrum has become less white) and the correlation times increase (the fluctuations develop long-term memory: a $1/f$ noise process has very large power at very long time lapses (very small ω) [13]).

To confirm this intuition, we computed the autocorrelation functions of the theoretical adiabatic spectra shown in Fig. 4. This was done numerically by converting each single-sided spectrum to a dc-centered, double-sided spectrum, applying a Hanning window, then taking the absolute value of its discrete inverse Fourier transform (using MATLAB's `abs` and `ifft` functions). As expected, the resulting autocorrelation graphs showed an exponential decay from a peak at zero lag. The decay time T was determined as the negative of the inverse slope of the semilogarithmic plot of autocorrelation versus lag time.

The predicted variation of correlation time T as a function of the anesthetic effect λ is shown in Fig. 9.

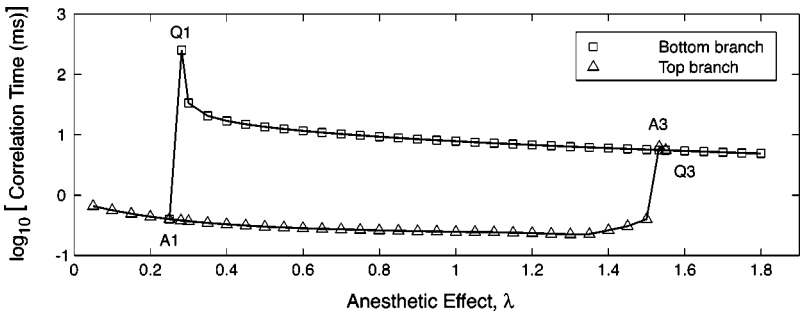

FIG. 9. Predicted variation of the correlation time for stochastic fluctuations as a function of λ. The correlation time is the 1/*e* decay time of the theoretical autocorrelation functions (Fourier transform of adiabatic fluctuation spectra of Fig. 4). Correlation times are plotted on a logarithmic scale. Note the apparent mirror symmetry (about the horizontal axis) with the spectral entropy curves of Fig. 7(a).

Comparison with Fig. 7(a) shows a remarkable mirror symmetry between correlation time and spectral entropy. The symmetry is not perfect, as can be seen from Fig. 10(b) where we plot spectral entropy versus correlation time on a logarithmic *x* scale. But, as a rough fit by eye would suggest, it would not be unreasonable to draw a straight line of negative slope through the points, indicating that, to first approximation, the spectral entropy *H* scales as the negative logarithm of the correlation time *T*.

This intriguing result motivated the following line of reasoning: The adiabatic macrocolumn has a fluctuation spec trum which is *nearly* Lorentzian, and for which it is *nearly* true to say $H \propto -(\ln T)$. So, could it be the case that for an ideal Lorentzian process this relation is exactly correct? We find that the answer is ''yes,'' and a proof for this claim is presented in the Appendix. We find that for an ideal Lorentzian of correlation time *T*, the unnormalized and normalized spectral entropies are given, respectively, by

$$H = -\ln T \quad \text{(unnormalized)}, \tag{3.5a}$$

$$H' = -\frac{1}{\ln f_{\max}} \ln T \quad \text{(normalized on } 0 < f < f_{\max}\text{)} \tag{3.5b}$$

for spectra plotted in linear frequency space (f: Hz). If the spectra are plotted in angular frequency space (ω: rad/s), then T is replaced by $2\pi T$ in these formulas, and $f_{\max}$ becomes $\omega_{\max}$ in Eq. (3.5b). See the Appendix for details.

IV. DISCUSSION

Although our adiabatic theory for the anesthetic-induced phase transition is based on the mean-field model of a single macrocolumn, it has been able to predict the following EEG behaviors that have been observed in clinical or laboratory settings.

(1) If the conscious → unconscious transition is a first-order phase change from a less-ordered to a more-ordered state, then there should be a ''latent heat'' effect: a sudden energy release to compensate for the loss of thermodynamic entropy. This prediction and its apparent corroboration in an experiment by Stullken *et al.* [14] was discussed in [2].

(2) Total EEG power should increase strongly as the induction point is approached, then decrease following induction; a similar power surge should occur at emergence (the ''biphasic'' effect [6–8,15]).

(3) Spectral energy should redistribute from higher to lower frequencies during induction, with the spectrum becoming increasingly narrow and dc-peaked [6]. This trans-

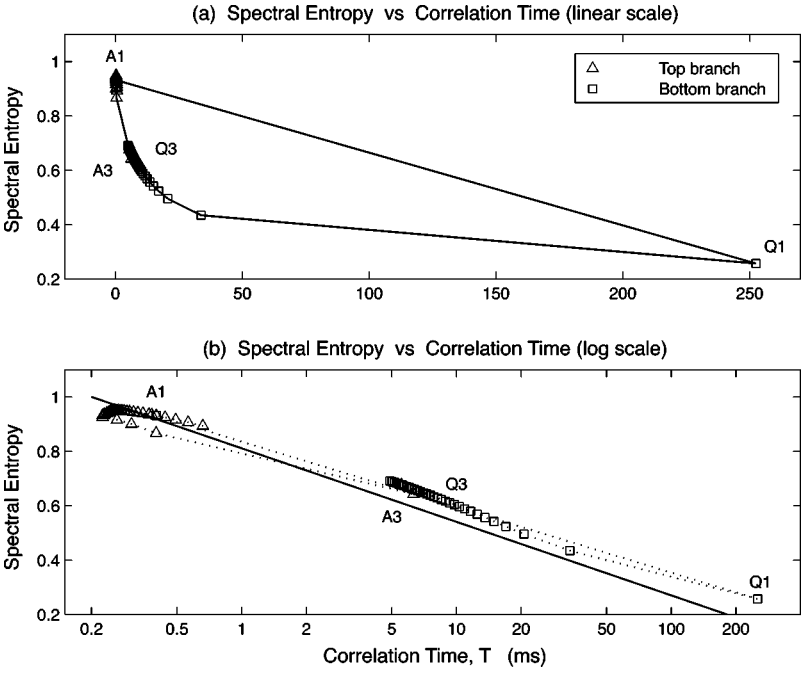

FIG. 10. Spectral entropy versus correlation time for the adiabatic model. (a) has a linear *x* scale to allow visual separation of the induction ($A_1A_3Q_3$) and emergence ($Q_3Q_1A_1$) trajectories. (b) Plotted with a logarithmic *x* scale, both trajectories merge, demonstrating an approximately linear relationship between spectral entropy and the logarithm of correlation time over three decades in *T*. The solid line in the lower graph is the $H' = -\ln T/\ln 5001$ prediction for *T* (in seconds) for an ideal Lorentzian process (see the Appendix for details).

formation from an approximately ''white'' spectrum to a $1/f$ ''colored'' spectrum should produce measurable reductions in spectral entropy [3].

Section III D of the present paper showed that spectral entropy is expected to be inversely related to the correlation time of the EEG voltage fluctuations. If this is true, then it suggests an alternative means of detecting the onset of transition: the EEG correlation times should increase strongly as the point of transition is approached. This should occur for both the induction into unconsciousness and for the reemergence into wakefulness. In order to test this prediction, care will need to be taken to ensure that any nonstochastic variations (e.g., α, θ, δ rhythms) are excluded from the analysis. Our simple adiabatic theory addresses only the stochastic component of the cortical signal, and is silent with respect to cortical resonances.

The work presented in this paper and its companion paper [2] raises two significant questions: (i) What is the relationship between anestheto-dynamic entropy S and spectral entropy H for the anesthetized cortex? and (ii) can these macroscopic entropies provide insight into an underlying statistical entropy which counts cortical microstates? We intend to address both questions in future work.

ACKNOWLEDGMENT

We wish to thank Dr. Hanna Viertiö-Oja for communicating her spectral entropy results to us, and for supplying the clinical data shown in Fig. 8.

APPENDIX A: SPECTRAL ENTROPY FOR A LORENTZIAN SPECTRUM

Consider the prototypical Lorentzian spectrum

$$\mathcal{S}(\omega)=\frac{1}{k^2+\omega^2},\quad 0<\omega<\infty \tag{A1}$$

whose decay rate k sets the half-power or -3-dB frequency. We convert the spectrum to a spectral probability distribution $p(\omega)$ by normalizing with respect to total spectral area,

$$p(\omega)=\frac{\mathcal{S}(\omega)}{\int_0^\infty \mathcal{S}(\omega)d\omega}\ \text{ so that }\ \int_0^\infty p(\omega)d\omega=1. \tag{A2}$$

The spectral area for the Lorentzian distribution is

$$\int_0^\infty \mathcal{S}(\omega)d\omega=\int_0^\infty \frac{d\omega}{k^2+\omega^2}=\frac{1}{k}\tan^{-1}\left(\frac{\omega}{k}\right)\Bigg|_0^\infty=\frac{\pi}{2k} \tag{A3}$$

giving the Lorentzian probability density function

$$p(\omega)=\frac{2k}{\pi}\frac{1}{k^2+\omega^2}. \tag{A4}$$

The spectral entropy H is obtained by evaluating the negative of the expectation value of $\ln p(\omega)$,

$$\begin{aligned}H&=-\int_0^\infty p(\omega)\ln p(\omega)d\omega\\&=-\int_0^\infty\frac{2k}{\pi}\frac{1}{k^2+\omega^2}\ln\left[\frac{2k}{\pi}\frac{1}{k^2+\omega^2}\right]d\omega\\&=-\frac{2k}{\pi}\left\{\ln\left[\frac{2k}{\pi}\right]\int_0^\infty\frac{d\omega}{k^2+\omega^2}-\int_0^\infty\frac{\ln[k^2+\omega^2]}{k^2+\omega^2}d\omega\right\}\\&=-\frac{2k}{\pi}\left\{\frac{\pi}{2k}\ln\left[\frac{2k}{\pi}\right]-I_1\right\}.\end{aligned} \tag{A5}$$

The value of the definite integral I_1 is tabulated (see formula 4.295.7 on p. 560 of [16])

$$I_1=\frac{\pi}{k}\ln 2k. \tag{A6}$$

This result allows us to write the spectral entropy H for the continuous Lorentzian spectrum in a simple closed form which depends only on k, the Lorentzian decay rate,

$$H=\ln(2\pi k). \tag{A7}$$

We see that the Lorentzian spectral entropy H exhibits the following limiting behaviors.

(1) $H\to+\infty$ as $k\to\infty$. As decay rate k increases, we approach the white-noise flat-spectrum limit in which energy is uniformly distributed over all frequencies, giving extreme maximum spectral entropy.

(2) $H=0$ when $k=1/2\pi$. If the spectrum is sufficiently jagged, its entropy can be zero, and a more jagged spectrum will have a negative entropy. This possibility of a negative continuous entropy is quite unlike the behavior of the discrete Shannon entropy of Eq. (3.1) which can never go negative.

(3) $H\to-\infty$ as $k\to0$. In this limit the Lorentzian distribution tends to the infinitely-peaked δ-function $\delta(\omega)$ which is zero everywhere except at zero frequency. For this delta-spike spectrum, spectral entropy reaches its extreme negative value.

Any real experiment involving a Lorentzian process will necessarily be band limited to some upper-limit frequency $\omega_{\max}$. In principle we could determine the spectral entropy of a band-limited Lorentzian by replacing ∞ by $\omega_{\max}$ in the integrals of Eqs. (A2) and (A5), but unfortunately the resulting expression for H cannot be integrated analytically and must be computed numerically.

An alternative approach to band limiting is to reference the entropy of the unlimited Lorentzian against the maximum entropy achievable on the band-limited domain $0<\omega<\omega_{\max}$. This suggests using a rectangular reference spectrum which is ''flat'' up to $\omega_{\max}$, and zero elsewhere,

$$\begin{aligned}p_{\text{rect}}(\omega)&=\frac{1}{\omega_{\max}},\quad 0<\omega<\omega_{\max}\\&=0,\quad \omega>\omega_{\max}\end{aligned}$$

and whose spectral entropy H_{rect} is

$$H_{\mathrm{rect}} = -\int_0^{\omega_{\max}} p_{\mathrm{rect}} \ln p_{\mathrm{rect}} d\omega = \ln \omega_{\max}. \tag{A8}$$

Thus we define a Lorentzian spectral entropy H' which has been normalized with respect to a band-limited rectangular reference,

$$H' = \frac{H}{H_{\mathrm{rect}}} = \frac{\ln(2\pi k)}{\ln \omega_{\max}}. \tag{A9}$$

With this normalization, $H'=1$ when $k=\omega_{\max}/2\pi$, meaning that for this value of decay rate k, the entropy of the open-ended Lorentzian matches that of a rectangular reference spectrum which is upper-band limited to $\omega_{\max}$.

In Figs. 7 and 10 in Sec. III of this paper, the spectral entropy calculations used frequencies f measured in Hz (rather than angular frequencies ω in rad/s). Applying the change of variable $\omega = 2\pi f$ to Eq. (A1) gives

$$\mathcal{S}(f) = \frac{1}{k^2 + (2\pi f)^2} = \frac{1/4\pi^2}{K^2 + f^2}, \tag{A10}$$

where $K = k/2\pi$, leading to a normalized band-limited spectral entropy

$$H' = \frac{\ln(2\pi K)}{\ln(N\Delta f)} = \frac{\ln k}{\ln(N\Delta f)} = \frac{\ln(1/T)}{\ln(N\Delta f)}, \tag{A11}$$

where $T = 1/k$ is the correlation time for the Lorentzian fluctuations. For the numerical experiment of Fig. 10, we set $\Delta f = 1$ Hz and $N = 5001$.

[1] M. L. Steyn-Ross, D. A. Steyn-Ross, J. W. Sleigh, and D. T. J. Liley, Phys. Rev. E **60**, 7299 (1999).

[2] M. L. Steyn-Ross, D. A. Steyn-Ross, J. W. Sleigh, and L. C. Wilcocks, preceding paper, *ibid.* **64**, 011917 (2001).

[3] H. E. Viertiö-Oja *et al.*, J. Clin. Monit. Comput. **16**, 60 (2000).

[4] C. W. Gardiner, *Handbook of Stochastic Methods for Physics, Chemistry, and the Natural Sciences*, Springer Series in Synergetics Vol. 13 (Springer-Verlag, Berlin, 1985).

[5] H. Risken, *The Fokker–Planck Equation: Methods of Solution and Applications*, Springer Series in Synergetics Vol. 18 (Springer-Verlag, Berlin, 1984).

[6] K. Kuizenga, C. J. Kalkman, and P. J. Hennis, Br. J. Anaesth. **80**, 725 (1998).

[7] M. B. MacIver, J. W. Mandema, D. R. Stanski, and B. H. Bland, Anesthesiology **84**, 1411 (1996).

[8] M. Bührer *et al.*, Anesthesiology **77**, 226 (1992).

[9] M. Steriade, D. A. McCormick, and T. J. Sejnowski, Science **262**, 679 (1993).

[10] C. E. Shannon and W. Weaver, in *The Mathematical Theory of Information* (University of Illinois Press, Urbana, IL, 1949).

[11] R. Q. Quiroga, J. Arnhold, K. Lehnertz, and P. Grassberger, Phys. Rev. E **62**, 8380 (2000).

[12] S. R. Shenoy, in *Stochastic Processes Formalism and Applications*, edited by G. S. Agarwal and S. Dattagupta, Lecture Notes in Physics Vol. 184 (Springer-Verlag, Berlin, 1983), pp. 238–244.

[13] B. R. Frieden, *Physics from Fisher Information: A Unification* (Cambridge University Press, Cambridge, UK, 2000).

[14] E. H. Stullken, Jr., J. H. Milde, J. D. Michenfelder, and J. H. Tinker, Anesthesiology **46**, 28 (1977).

[15] D. P. Archer and S. H. Roth, Br. J. Anaesth. **79**, 744 (1997).

[16] I. S. Gradshteyn and I. M. Ryzhik, *Table of Integrals, Series, and Products* (Academic Press, New York, 1965).

[17] H. Viertiö-Oja, Anesthesiology News **26(4)**, 1 (2000).